

CHARACTERIZATION OF DISTURBANCES IN THE SPACE ENVIRONMENT FOR AUTONOMOUS CLOSE-RANGE RENDEZVOUS OF COOPERATIVE ROBOTS

Josue D. Muñoz^a
jdm03@ufl.edu

Gloria J. Wiens^b
gwiens@ufl.edu

University of Florida, Department of Mechanical and Aerospace Engineering, Space, Automation, and Manufacturing Mechanisms Laboratory, 231 MAE-A P.O. Box 116250, Gainesville, FL. 32611-6250.

The topic of autonomous close-range rendezvous is discussed in this paper. When designing a controller for an autonomous system, it is important to model the environment of the system as precisely as possible. This paper discusses the disturbances encountered in space and their effects on the rendezvous controller with particular focus on the effects in fuel usage and mission times. Simulations are performed for two scenarios: near circular low-Earth orbits and eccentric geosynchronous orbits. It was found that disturbances affected the controller for the eccentric geosynchronous orbits considerably more than that found for near circular low-Earth orbits, which largely can be attributed to aerodynamic drag experienced at periapsis.

I. INTRODUCTION

There is currently an effort to develop autonomous cooperative robots for on-orbit services. These services include but are not limited to: docking, space tug/orbital life extension, refuel or recharge/replace battery, sensing/inspection/surveillance, repair/replace parts, and on-orbit assembly. In order to perform all these operations it is necessary for the vehicle performing the services (chaser) to rendezvous with the vehicle being serviced (target).

This brings up the question: “What classifies rendezvous?” Rendezvous can be bifurcated into two categories: far-range and close-range⁴. Far-range rendezvous occurs after the chaser is inserted into a coplanar orbit with the target. It consists of minimizing the phase and range (~ 10 km) between the chaser and target. Close-range rendezvous occurs after far-range rendezvous and consists of minimizing the range further (< 1 km). It will be assumed that the chaser and target are in near coplanar orbits and in close-range, and that the close-range rendezvous process will be achieved autonomously.

When modeling the environment, two fundamental disturbances will be included: J2 effects and aerodynamic drag. The rendezvous controller tested will be based on the Artificial Potential Function Guidance (APFG)⁶.

II. SYSTEM DYNAMICS

Each vehicle will be modeled using the nonlinear equation of motion describing the classical two-body problem¹:

$$\ddot{\underline{r}} + \frac{\mu}{r^3} \underline{r} = \underline{a}_d \quad (1)$$

where \underline{r} is the position of the vehicle measured from the Earth’s center, μ is the gravitational parameter of the Earth, and \underline{a}_d is the disturbing acceleration on the vehicle.

The relative position between the two vehicles will be defined as:

$$\delta \underline{r} = \underline{r}_c - \underline{r}_t \quad (2)$$

where \underline{r}_c is the position of the chaser and \underline{r}_t is the position of the target.

When considering the disturbing acceleration to be zero, the solution to the two-body problem is known and can be written in the form¹:

$$\begin{aligned} \underline{r} &= \underline{r}(\underline{\alpha}, t) \\ \underline{v} &= \underline{v}(\underline{\alpha}, t) \end{aligned} \quad (3)$$

where \underline{v} is the velocity vector, and $\underline{\alpha}$ is a set of constant orbital elements that describe the orientation and shape of the orbit and the position in the orbit. It should be noted that there exists many different sets of orbital elements. However, the set used in this paper are the “classical orbital elements”¹:

$$\underline{\alpha} = [a \quad e \quad \Omega \quad i \quad \omega \quad f] \quad (4)$$

where a is the semi-major axis, e is the eccentricity, Ω is the longitude of the ascending node, i is the

inclination, ω is the argument of periapsis, and f is the true anomaly.

When the disturbing accelerations are introduced, these orbital elements are no longer constant. The differential equation of the orbital elements can be found as a function of the magnitude of the disturbing acceleration using the variation of parameters technique¹.

Also, given the position and velocity vector, the orbital elements can be determined using a basic algorithm². The physical description of each orbital element will be shown in the following section.

II.A. Coordinate Transformations

There are four coordinate systems that must be discussed. The Perifocal coordinate system (PQW) is the easiest coordinate system to describe an orbit. To describe the orientation of the orbit relative to the Earth, the Earth-Centered Inertial system (ECI) is used. The Local Vertical Local Horizon (LVLH), or local osculating polar coordinate system, is useful when describing relative motion. The intrinsic coordinate system is particularly useful to describe the aerodynamic drag since drag acts along the direction of the velocity².

II.A.1. Perifocal Coordinate System (PQW)

The origin of the Perifocal system is taken to be the center of the Earth. The first direction is defined by the direction of the periapsis. The third direction is defined by the vector normal to the orbital plane. Consequently, the second direction is defined by the cross product between the first direction and the third direction².

The coordinate system is illustrated in Fig. 1 where \hat{P} is to the right, \hat{Q} is upward, and \hat{W} is out of the page. The figure also shows how the semi-major axis, eccentricity, and true anomaly are defined for the orbit.

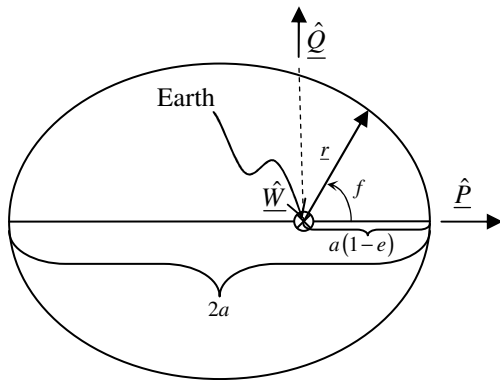


Fig. 1. Description of Perifocal coordinate system and semi-major axis, eccentricity, and true anomaly.

II.A.2. Earth-Centered Inertial Coordinate System (ECI)

The origin of the ECI coordinate system is taken to be the center of the Earth. The Perifocal coordinate system can be obtained from the ECI coordinate system by a 3-1-3 Euler sequence²

$$\underline{\underline{C}}_{IJK}^{PQW} = \underline{\underline{C}}_3(\omega)\underline{\underline{C}}_1(i)\underline{\underline{C}}_3(\Omega) \quad (5)$$

where $\underline{\underline{C}}_i$ denotes a rotation about the i^{th} axis.

The ECI coordinate system's first direction is defined in the direction of the vernal equinox. The third direction is defined by the North Pole. Consequently, the second direction is defined by the cross product of the third direction and the first direction.

Fig. 2 illustrates how the longitude of the ascending node, inclination, and argument of the periapsis relate the Perifocal coordinate system and the ECI coordinate system.

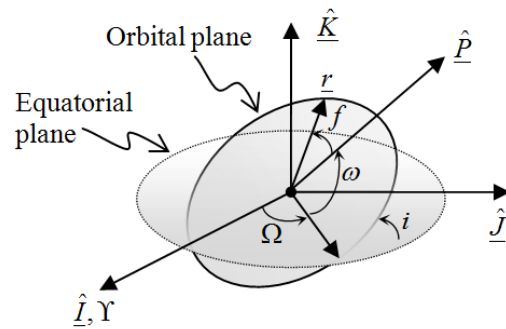


Fig. 2. Description of Earth-Centered Inertial system and longitude of ascending node, inclination, and argument of periapsis.

II.A.3. Local Vertical Local Horizon Coordinate System (LVLH)

The LVLH coordinate system has its origin at the vehicle's center of mass and can be defined from the Perifocal coordinate system by a coordinate transformation about the third axis².

$$\underline{\underline{C}}_{PQW}^{LVLH} = \underline{\underline{C}}_3(f) \quad (6)$$

Fig. 3 illustrates how the local osculating polar coordinate system (LVLH) is defined. It should be noted that the position is along the \hat{x} direction but the velocity of the vehicle is not always along the \hat{y} direction; especially for eccentric orbits. Therefore it is important to define an intrinsic coordinate system.

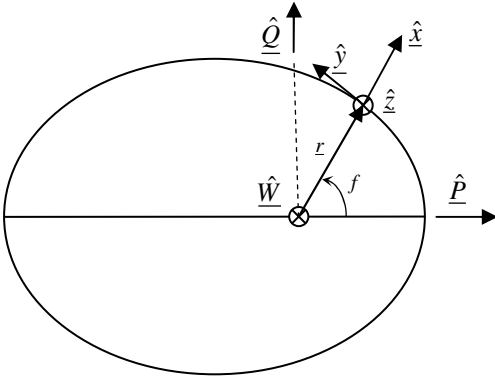


Fig. 3. Description of local osculating polar coordinate system as it relates to the Perifocal coordinate system.

II.A.4. Intrinsic Coordinate System

The intrinsic coordinate system has its origin at the vehicle's center of mass and is defined as follows:

$$\underline{e}_t = \frac{\underline{v}}{v} \quad \underline{e}_n = \frac{\frac{d\underline{e}_t}{dx}}{\left\| \frac{d\underline{e}_t}{dx} \right\|} \quad \underline{e}_b = \underline{e}_t \times \underline{e}_n \quad (7)$$

where v is the magnitude of the velocity vector and can be calculated as follows¹:

$$v = \sqrt{\mu \left(\frac{2}{r} - \frac{1}{a} \right)} \quad (8)$$

The intrinsic coordinate system can also be obtained directly by a coordinate transformation on the LVLH coordinate system¹

$$\underline{C}_{LVLH}^{INT} = \frac{h}{pv} \begin{bmatrix} e \sin(f) & -1 - e \cos(f) & 0 \\ 1 + e \cos(f) & e \sin(f) & 0 \\ 0 & 0 & 1 \end{bmatrix} \quad (9)$$

where p is known as the parameter, h is the magnitude of the angular momentum vector and both can be found as follows¹:

$$p = a(1 - e^2) \quad (10)$$

$$h = \sqrt{p\mu}$$

It should be noted that since these parameters are functions of the orbital elements, then they are also variable when a disturbing acceleration is present.

II.B. Disturbances

There are many disturbances that occur in space. To name a few these are: Earth's oblateness (J2) effects, aerodynamic drag, third body (Sun, Moon, Jupiter, etc.) gravity effects, solar radiation pressure, and thrusts applied to body².

II.B.1. J2 Effect

The J2 effect arises when the Earth is no longer considered a spherically homogeneous mass. As a result the Earth is divided into spherical harmonic surfaces^{1,2}. The second zonal harmonic (J2) provides by far the strongest disturbing acceleration on a body orbiting the Earth. This disturbing acceleration can be described in the LVLH frame as⁵

$$\underline{a}_{J2} = -\frac{3}{2} J_2 \mu \frac{R_{\oplus}^2}{r^4} \left[\begin{aligned} & [1 - 3 \sin^2(i) \sin^2(\theta)] \underline{x} + \\ & 2 \sin^2(i) \sin(\theta) \cos(\theta) \underline{y} + \\ & 2 \sin(i) \cos(i) \sin(\theta) \underline{z} \end{aligned} \right] \quad (11)$$

Here R_{\oplus} is the radius of the Earth and

$$J_2 = 0.0010826 \quad (12)$$

$$\theta = \omega + f$$

where J_2 is the second zonal harmonic constant, and θ is known as the argument of latitude.

II.B.2. Aerodynamic Drag

The drag experienced by the vehicle depends on the geometry of the vehicle and the altitude. The disturbing acceleration due to drag can be defined as¹

$$\underline{a}_{drag} = -C \rho v^2 \underline{e}_t \quad (13)$$

Here C is the ballistic coefficient which is defined as

$$C = \frac{m}{c_d A} \quad (14)$$

where m is the mass of the vehicle, c_d is the drag coefficient, and A is the average cross-sectional area of

the vehicle. The values used for these parameters are shown in Table I.

TABLE I. Physical parameters of each vehicle.

Parameter	Value
m	100 kg
c_d	2.2
A	25 m ²

To obtain an accurate disturbing acceleration for drag, the air density is modeled as a function of height as follows¹:

$$\rho(h) = \rho_0 \exp\left(-\frac{(r - R_{\oplus}) - q}{H}\right) \quad (15)$$

where ρ_0 is the reference density, q is the reference height, and H is the scale height. Values for these parameters depend on the height of the vehicle as well and are tabulated³.

II.C. Controller

Autonomous control for guidance of space systems is a topic that recently is receiving much greater attention within the research and development community. When designing one of these controllers it is important to consider three factors: fuel expenditure, control law, and computational efficiency. It is important to conserve fuel because supply is limited, and once depleted refueling is virtually not possible. The control law for the rendezvous lends to this as well. Continuous actuation could be used in space, however, impulsive actuation is more fuel efficient. Thus it is important to consider a control law that provides impulsive control inputs. Computational efficiency is also very important if autonomous guidance and control is to be performed on-board. Space-certified hardware does not have the ability to compute complex algorithms real-time. Thus it is important that the control algorithm be simple yet satisfies the other two constraints.

The controller chosen for this paper is known as Artificial Potential Function Guidance (APFG)⁶. This controller was chosen because it satisfies the latter two constraints. Fuel usage could be somewhat optimized by heuristics or other methods.

First a Lyapunov function will be defined by as a function of the relative position of the chaser to the target.

$$V = \delta \underline{r}^T \delta \underline{r} \quad (16)$$

The control law is defined as:

$$\underline{a}_T = \begin{cases} \underline{0} & \text{if } \dot{V} < 0 \\ \frac{\Delta \underline{v}}{\Delta t} & \text{if } \dot{V} \geq 0 \end{cases} \quad (17)$$

where \underline{a}_T is the disturbing acceleration from the thrust and Δt is the length of the burn and should be significantly small. The impulsive thrust by the chaser is $\Delta \underline{v}$ and is defined by the negative gradient of the Lyapunov function:

$$\Delta \underline{v} = -k \nabla_{\delta \underline{r}} V - \delta \dot{\underline{r}}^- \quad (18)$$

where k is a constant gain and $\delta \dot{\underline{r}}^-$ is the relative velocity of the chaser with respect to the target immediately before the impulse.

III. RESULTS

To test the effects of disturbances, two different types of orbits will be simulated: near circular low-Earth orbit (LEO) and an eccentric geosynchronous orbit (GEO). In each case, one run will be performed without the disturbances, and the other run will be performed with the J2 and aerodynamic disturbances.

Two constraints were also placed on the impulses. A maximum magnitude of 5 m/s per impulse was allowed and consecutive impulses cannot occur within 20 seconds of each other. The value used for the constant gain used in the control law was 10^{-4} .

III.A. Near Circular LEO

The set of orbital elements that describes a near circular LEO for the chaser is shown in Table II. Table III shows the difference in orbital elements between the chaser and target. The orbit is illustrated to scale in Fig. 4. It should be noted that the difference between the chaser's orbit and the target's orbit cannot be seen at this scale.

TABLE II. Orbital elements for chaser (near circular LEO).

Orbital Element	Value
a	7500 km
e	0.02
Ω	120 deg
i	30 deg
ω	10 deg
f	20 deg

TABLE III. Orbital element difference between chaser and target. (near circular LEO)

Orbital Element	Value
Δa	-0.002 km
Δe	0.001
$\Delta \Omega$	0 deg
Δi	0.005 deg
$\Delta \omega$	0 deg
Δf	0 deg

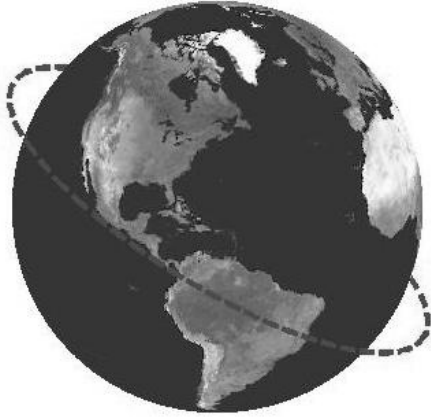


Fig. 4. Illustration of near circular LEO.

III.A.1. Neglecting Disturbances

The relative position and relative velocity of the chaser with respect to the target is shown in Fig. 5.

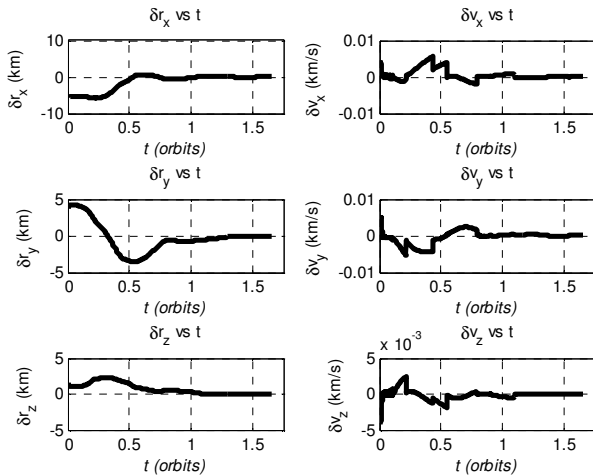


Fig. 5. Relative position and relative velocity (near circular LEO without disturbances).

Fig. 6 shows the history of the corresponding impulses from the chaser. There were 19 burns with a

total amount of $\Delta v = 29.59 \text{ m/s}$ and a mission time of 10664 seconds or 1.65 orbits.

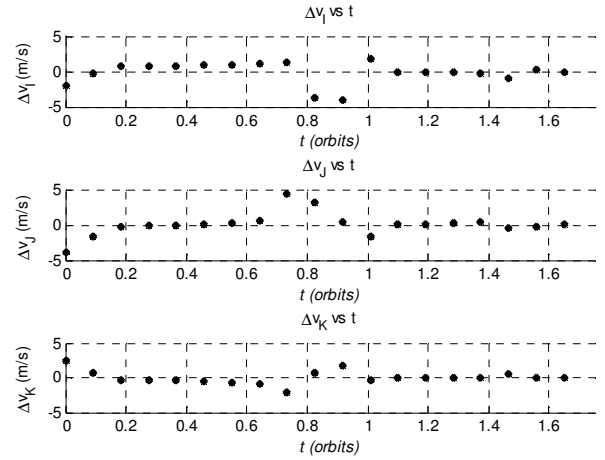


Fig. 6. Impulse history (near circular LEO without disturbances).

III.A.2. With Disturbances

The response and impulse history with the disturbances of the near circular LEO case looked much the same as without disturbances. Fig. 7 shows the magnitudes of the disturbances experienced by the target and chaser. Note that the scale on the chaser's disturbances is much larger because the magnitude of thrusts is much greater than the magnitude of the other disturbances.

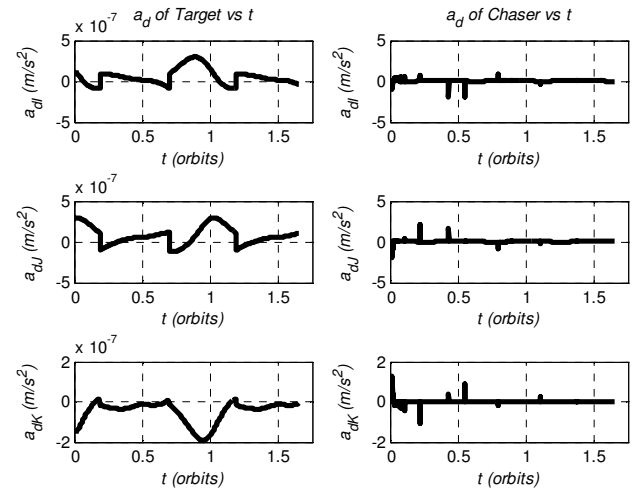


Fig. 7. Disturbances experienced by target and chaser (near circular LEO).

There were 19 burns with a total amount of $\Delta v = 29.60 \text{ m/s}$ and a mission time of 10664 seconds or 1.65 orbits.

III.B. Eccentric GEO

The set of orbital elements that describes an eccentric GEO for the chaser is shown in Table IV. Table V shows the difference in orbital elements between the chaser and target. The orbit is illustrated to scale in Fig. 8. It should be noted that the difference between the chaser's orbit and the target's orbit cannot be seen at this scale.

TABLE IV. Orbital elements for chaser. (eccentric GEO)

Orbital Element	Value
a	36,000 km
e	0.5
Ω	120 deg
i	70 deg
ω	30 deg
f	20 deg

TABLE V. Orbital element difference between chaser and target. (eccentric GEO)

Orbital Element	Value
Δa	-2 km
Δe	-0.001
$\Delta \Omega$	0 deg
Δi	0.05 deg
$\Delta \omega$	0 deg
Δf	0 deg

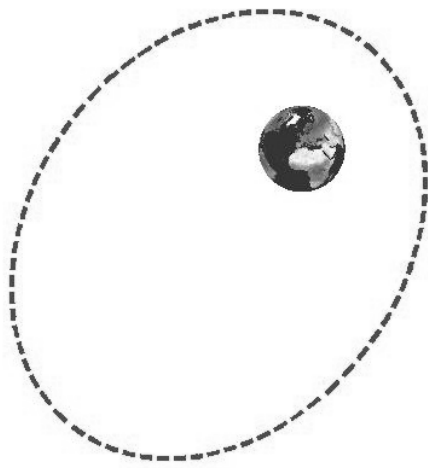


Fig. 8. Illustration of eccentric GEO.

III.B.1. Neglecting Disturbances

The relative position and relative velocity of the chaser with respect to the target is shown in Fig. 9.

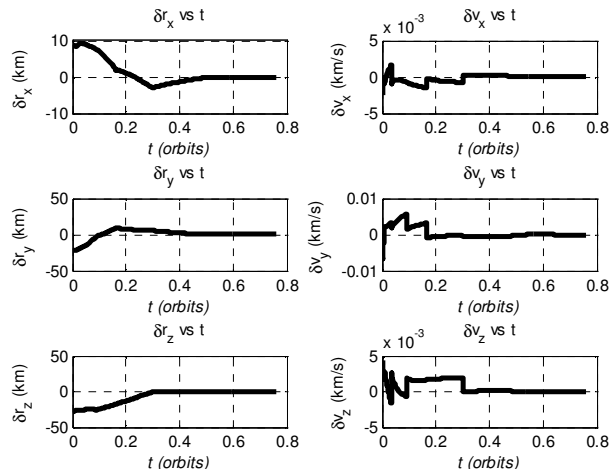


Fig. 9. Relative position and relative velocity history (eccentric GEO without disturbances).

Fig. 10 shows the history of impulses from the chaser. There were 8 burns with a total amount of $\Delta v = 23.51 \text{ m/s}$ and a mission time of 51602 seconds or 0.76 orbits.

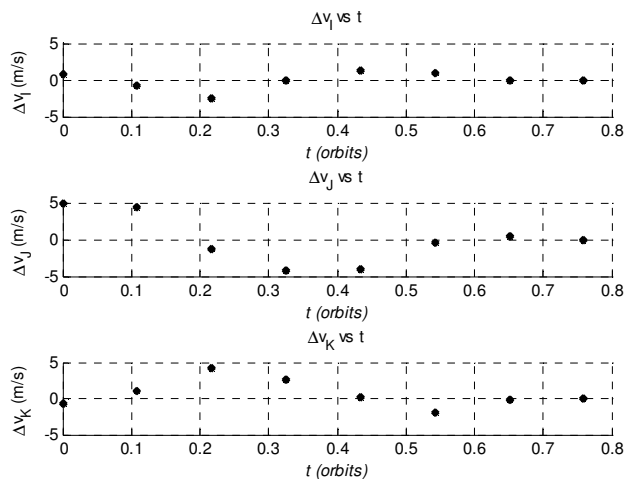


Fig. 10. Impulse history (eccentric GEO without disturbances).

III.B.2. With Disturbances

Fig. 11 shows the magnitudes of the disturbances experienced by the target and chaser. Note that the scale for the disturbances is much larger now; particularly,

when both vehicles are initially near the periapsis. Since both are also in eccentric orbits, their velocities are much faster and as a result the aerodynamic drag has a much greater effect.

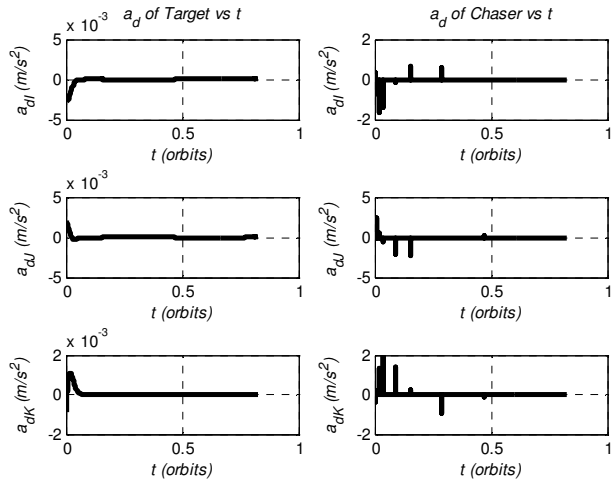


Fig. 11. Disturbances experienced by target and chaser (eccentric GEO) .

The relative position and relative velocity of the chaser with respect to the target is shown in Fig. 12.

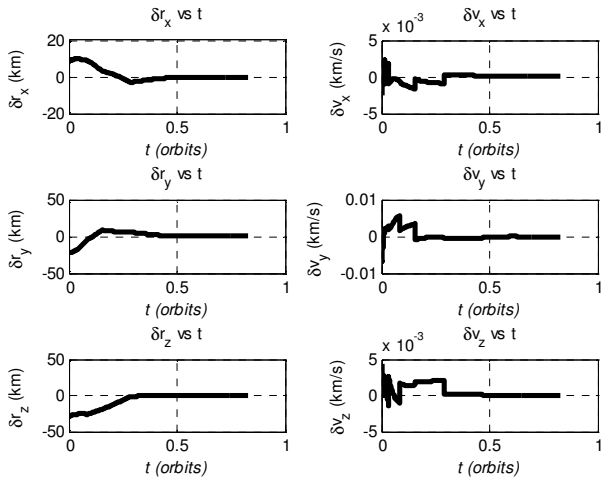


Fig. 12. Relative position and relative velocity history (eccentric GEO).

Fig. 13 shows the history of impulses from the chaser. There were 10 burns with a total amount of $\Delta v = 27.56 \frac{m}{s}$ and a mission time of 56110 seconds or 0.83 orbits.

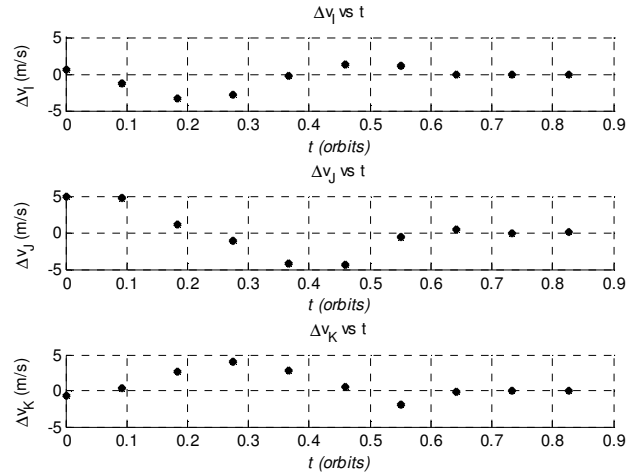


Fig. 13. Impulse history (eccentric GEO).

IV. CONCLUSIONS

Focusing on the effects of fuel usage and mission times, this paper discusses the disturbances encountered in space and their effects on the rendezvous controller. Simulations results show that the effect of disturbances was negligible for near circular LEO. However, when considering eccentric GEOs the disturbances did increase the Δv by 4 m/s and the mission time by close to 4500 seconds. It was inferred that this was largely due to the fact that initially both vehicles were near the periapsis, and as a result had greater velocities.

REFERENCES

1. R. H. Battin. *An Introduction to the Mathematics and Methods of Astrodynamics*, AIAA, Reston, VA 1999.
2. D. A. Vallado. *Fundamentals of Astrodynamics and Applications*, Microcosm Press and Kluwer Academic Publishers, El Segundo, California and Dordrecht/Boston/London 2001.
3. J. R. Wertz. *Spacecraft Attitude Determination and Control*, Kluwer Academic Publishers, Dordrecht/Boston/London 1988.
4. W. Fehse. *Automated Rendezvous and Docking of Spacecraft*, Cambridge University Press, Cambridge, UK 2003.
5. S.A. Schweighart, R.J. Sedwick. "High-Fidelity Linearized J_2 Model for Satellite Formation Flight," *AIAA Journal of Guidance, Control, and Dynamics*, Vol. 25, No. 6, pp. 1073-1080 (2002).
6. I. Lopez, C. R. McInnes. "Autonomous Rendezvous Using Artificial Potential Function Guidance," *AIAA Journal of Guidance, Control, and Dynamics*, Vol. 16, No. 2, pp. 231-241 (1995).